Int J Appl Earth Obs Geoinformation 88 (2020) 102083

Contents lists available at ScienceDirect

Int J Appl Earth Obs Geoinformation

journal homepage: www.elsevier.com/locate/jag

# MAPPING VEGETATION COMMUNITIES INSIDE WETLANDS USING SENTINEL-2 IMAGERY IN IRELAND

Saheba Bhatnagar[a], Laurence Gill[a], Shane Regan[c], Owen Naughton[d], Paul Johnston[a], Steve Waldren[b], Bidisha Ghosh[a,*]

[a] Trinity College Dublin, Department of Civil, Structural and Environmental Engineering, Ireland
[b] Trinity College Dublin, School of Natural Sciences, Ireland
[c] National Parks and Wildlife Survey, Ireland
[d] Institute of Technology Carlow, Department of the Built Environment, Ireland

ARTICLE INFO

*Keywords:*
Vegetation classification
eco-hydrology
spectral analysis
edge detection
bagged tree
image segmentation
graph cut
maximum-a-posteriori estimation

ABSTRACT

Wetlands provide habitat for a wide variety of plant and animal species and contribute significantly to overall biodiversity in Ireland. Despite these known ecosystem services, the total wetland area in Ireland has reduced significantly over the past few decades leading to an ongoing need to protect such environments. The EU Habitats Directive (92/43/EEC) has recognised several wetlands types as "priority" habitats. This study concentrates on a subset of the priority habitats focussing on some groundwater dependent terrestrial ecosystems, (in particular calcareous fens and turloughs), as well as raised bogs. Monitoring these sites across the country by field visits is resource-intensive. Therefore, this study has evaluated remote sensing as a potentially cost-effective tool for monitoring the ecological health of the wetlands. Identification and presence of certain vegetation communities can indicate the condition of the wetland, which can be used for monitoring, for example, activities causing degradation or the progress of restoration attempts. The ecological composition of the wetlands has been analysed using open-source Sentinel-2 data. 10 bands of Sentinel-2 Level-2 data and 3 indices, Normalised Difference Vegetation Index (NDVI), Enhanced Vegetation Index (EVI) and Normalised Difference Water Index (NDWI) were used to create vegetation maps of each wetland using Bagged Tree (BT) ensemble classifier and graph cut segmentation also known as MAP (maximum a *posteriori*) estimation. The proposed methodology has been validated on five raised bogs, five turloughs, and three fens at different times during 2017 and 2018 from which three case studies are presented. An overall classification accuracy up to 87% depending on the size of the vegetation community within each wetland has been achieved which suggests that the proposed method is appropriate for wetland health monitoring.

## 1. Introduction

Wetlands, both natural and man-made, comprise approximately one-quarter of the total area of Ireland (Ireland's Wetlands, 2000). They are known to provide a critical function concerning climate change, biodiversity, hydrology, and human health (Ramsar Convention Bureau, 2001). Despite these known ecosystem services, the total wetland area in Ireland (as well as globally) has reduced significantly (more than 10%) over the past few decades due to human interference (Maltby and Acreman, 2011). "Priority" habitats such as Active Raised Bog (ARB), Calcareous fens (CF) and Turloughs occur throughout the midlands and west of Ireland (Felicity Hayes-McCoy, 2017). It is estimated that raised bogs once spread across an area of more than 300,000 hectares. Unfortunately, due to decades of turf cutting and associated drainage used to fuel power plants, household fuel, compost, etc., only approximately 18,000 hectares of these wetlands remain. Hence, there is a pressing need for protecting such sites in Ireland.

In response to pressures related to land management, climate change and impacts from restoration activities, etc., ecological monitoring of the wetlands is necessary. However, ecological surveys are difficult to carry out due to the limitations in socio-economical resources, and the often secluded location of the habitats. Due to this, remote sensing (RS), with its increasing use in wider eco-hydrological applications, is becoming a more commonly utilised tool for the identification and classification of wetlands (Mahdavi et al., 2018).

Previous RS studies carried out on wetlands have mainly focused on

* Corresponding author.
*E-mail address:* bghosh@tcd.ie (B. Ghosh).

https://doi.org/10.1016/j.jag.2020.102083
Received 2 August 2019; Received in revised form 30 January 2020; Accepted 5 February 2020
Available online 14 February 2020

**Table 1**
Description of wetlands used in the study.

| | Wetland | Wetland description | Name | Location | County | Area(ha) |
|---|---|---|---|---|---|---|
| 1 | Raised bog | Discrete, dome-shaped masses of peat occupying former lakes or shallow depressions. The ecological health of the bog can be determined by the nature of its surface vegetation community composition (termed ecotopes) in relation to its water table and topography. | Clara | 53.327, -7.620 | Offaly | 250 |
| | | | Mongan | 53.320, -7.950 | Offaly | 205 |
| | | | Monivea | 53.361, -8.680 | Galway | 160 |
| | | | Killyconny | 53.789, -6.969 | Meath | 191 |
| | | | Knockacollar | 53.969, -7.539 | Laois | 130 |
| 2 | Calcareous fen | Peaty habitats, often fed by precipitation, groundwater and surface water (Goodall and Gore, 1983). These wetlands are continually wet and rich in biodiversity (Kimberley and Coxon, 2013). | Scragh bog | 53.579, -7.360 | Westmeath | 22.8 |
| | | | Toryhill | 52.538, -8.686 | Limerick | 0.95 |
| | | | Ballymore | 53.494, -7.637 | Westmeath | 11 |
| 3 | Turloughs | Depressions in karst areas, seasonally flooded mostly by groundwater. The ephemeral inundation plays a big role in the biological diversity of the turloughs (Naughton et al., 2012).When dry, have a grassy appearance due to presence of sedges, with a gradation of communities down into the lower part of the turlough basin (where water is sustained the longest) to more wetland associated species such as small sedges, silverweed, and meadowsweet (Irish Wetlands Type, 2018). | Blackrock | 58.121, -8.741 | Galway | 143 |
| | | | Knockaunroe | 52.988, -9.032 | Clare | 42.5 |
| | | | Turloughmore | 54.066, -8.692 | Clare | 21 |
| | | | Roo West | 53.967, -8.917 | Galway | 28 |
| | | | Lough Aleennaun | 53.007, -9.118 | Clare | 10.7 |

mapping and distinguishing the different types of wetlands in the form of peatlands, marsh, swamp, bog, fen, etc. The study by Grenier et al. (2008) used SPOT-4 images for categorising the area in 6 main wetland types. Combining both optical and SAR, a study by Mahdavi et al. (2019) effectively classified wetlands in 5 different locations. In Ireland, similar studies (Connolly, 2019; Nitze et al., 2015) have mapped Irish wetlands using optical data. However, to date, few studies have carried out detailed community mapping inside the wetlands to determine their ecological conditions. The study by Lehmann et al. (2016) mapped sphagnum species in a peat bog along with dead vegetation and lichens using high-resolution images from an unmanned aerial system (UAS). Another study by Knoth et al. (2013) used visible and infrared images from two unmanned aerial vehicles (UAV) to map a bog complex. Apart from high-resolution images, free Landsat data has been used to accurately map 6 classes inside a raised bog (Crichton et al., 2015). Sentinel-2 (S2) time series data was used by Rapinel et al. (2019) to map 7 broad communities in a grassland. The authors have mapped 5 vegetation communities in a single raised bog in Ireland (Bhatnagar et al., 2018). The aforementioned studies and other available literature mainly focussed on communities identified within a single wetland type. In this study, we have developed a generalised methodology for detailed mapping of vegetation communities present within multiple types of wetlands. Instead of expensive but high-resolution UAV data, the study was implemented using time series of freely available Sentinel-2 data. The methodology can be applied to all types of wetlands and has been tested on wetlands present in Ireland.

For detailed species mapping, studies (Förster et al. 2017; Koch et al., 2017) have often used support vector machine (SVM) to classify time-series S2 data. Studies carried out by Amani et al. (2017), Millard and Richardson (2015), and Nitze et al. (2015) depict the advantage of using ensemble classifiers for wetland classification. Studies like Amani et al. (2019a) have also used ensemble classifier on 30,000 Landsat-8 images implemented using the new Google Earth Engine platform (GEE). GEE is a high-performance computational platform utilising satellite data gathered from various Earth observation (EO) sources and provides many advanced machine learning tools and wide-scope of inbuilt EO applications using the cloud. The GEE provides the opportunity to explore remote sensing for the wider population of scientists and engineers who may not necessarily be remote sensing experts (Mahdianpari et al., 2019). However, GEE is the most appropriate for large areas with open source, multi-temporal satellite data (Farda, 2017). A study done by Hird et al. (2017) for large area wetland mapping, applies boosted regression trees using GEE and multi-source satellite data. Other studies like Mahdianpari et al. (2019), Amani et al. (2019b) illustrates the usage of ensemble classifiers via GEE for Canadian wetland mapping at a large scale. The current GEE libraries are available in Python and JavaScript languages and the results can be exported and analysed separately (Gorelick et al., 2017). Other generic platforms based on language R, Python or MATLAB are also widely used which may provide more flexibility for remote sensing experts. The study done on Clara bog by the authors (Bhatnagar et al., 2018) illustrated the use of BT applied on pixels for mapping vegetation communities within the wetlands. Consequently, a comparative analysis between the state-of-the-art classifiers was performed. The ensemble method called **b**ootstrap **agg**regat**ing** aka Bagging Trees (BT) proved to be the best technique. Although effective, this technique tends to produce some spurious pixels compromising the accuracy of the map. A possible solution to overcome these errors is to partition the image into homogenous closed groups or segments based on proximity (area). Hence, pixels are no more a single entity but part of an enclosed segment. This study extends the BT classification results to form a basis for image segmentation using contextual information. Maximum-a-*posteriori* estimation commonly known as Graph Cut (GCut) segmentation has been used for final vegetation mapping using image segmentation. The overall customised combination of the aforementioned algorithms used to precisely map the vegetation communities is termed as the Mapping

Vegetation Communities (MVC) algorithm.

The study therefore presents a methodology and results of using the MVC algorithm on the satellite images to map vegetation communities in bog, fen, and turlough wetlands for multiple days between June 2017 and October 2018. The methodology presented can be followed for automatisation of the health monitoring of different wetlands over time which should be able to warn of progressive degradation or, alternatively progress in terms of restoration activities.

## 2. Wetland Description

Groundwater dependant terrestrial ecosystems (GWDTEs) include a wide range of wetlands, which are home to many endangered species (Kimberly and Coxon, 2013). This study concentrates mainly on two types of GWDTEs (see, Table 1) and raised bog wetlands. The later although not traditionally classified as GWDTEs require high water levels that may also be supported by the interaction between the water in the peat and the underlying regional groundwater (Regan et al., 2019). A total of 13 wetlands are mapped in this study consisting of 5 raised bogs, 5 turloughs, and 3 fens. These wetlands are located in the west and middle of Ireland, in over 6 different counties. The details of the wetlands are given in Table 1, with a further discussion on 3 specific case studies in Section 4.

## 3. Materials And Method

Sentinel-2 (S2) data was used to map vegetation communities on the wetlands by performing supervised classifications using the BT and image segmentation using MAP. The S2-level 2A bottom of atmosphere (BOA) reflectance images were used for multiple dates over two years (2017, 2018) and the results were verified using field derived vegetation maps. An overview of the workflow is shown in Fig. 1.

### 3.1. SENTINEL-2 DATA

The Sentinel-2 Multispectral Instrument Level 2A (S2-MSIL2A) images used are bottom-of-atmosphere (BOA) reflectance in cartographic geometry. The L2A-BOA product is atmospherically corrected and ready to use (ESA Sentinel online, 2000) and is accessed from the Copernicus Open Access Hub (Copernicus Open Access Hub, 2018). The areas that were used lie under tile IDs - T29UNV, T29UNU, T29UPV of Sentinel-2 footprints (Fig. 2). Pre-processing of the images was carried out using software SNAP v.6.0 ("SNAP - ESA Sentinel Application Platform") which includes resampling, sub-setting, up-sampling of the bands acquired at 20 m to obtain a stack of spectral bands at 10 m resolution.

S2 Level 2 has a total of 12 bands out of which 10 bands (Bands 2-8A and Bands 11-12) have been used for analysis in this study (Gatti and Bertolini, 2013) as shown in Table 2. These bands were chosen due to their spectral significance and compatible spatial resolutions.

The images used for all the wetlands analysed in this study were captured at multiple times throughout 2017 and 2018. For optimum analysis, only the cloud-free images were chosen which restricted the sample size. A total of 7 dates were selected where both the bogs and fens being studied were out of the impact of clouds. Since turloughs are flooded during the winters, only summer images were chosen for its analysis. The main reason for starting the study from 2017 was the availability of S2 Level-2 products with Level-2A (bottom of atmosphere reflectance) images only available from March 2017. The months for which the imagery was captured for bogs and fens are June 2017, December 2017, February 2018, April 2018, June 2018, July 2018, and October 2018. For turloughs, the non-inundated months were chosen which are June 2017, June 2018, and July 2018.

Along with the 10 spectral bands, 3 additional vegetation and water indices were used to enhance the classification process. The details about these indices are presented in Table 3.

### 3.2. Boundary Delineation

For mapping and monitoring the wetlands, a boundary delineation algorithm was applied, as detailed in Bhatnagar et al. (2018), using NDVI as the base image ($B_i$) to separate wetlands from non-wetland areas (see Fig. 3). The satellite image was delineated using a combination of three edge detection and segmentation techniques namely entropy filtering (Vázquez et al., 1999), canny edge detection (Canny, 1987) and lazy snapping (Li et al., 2004). Entropy filtering and canny edge detection techniques initially highlight the edges of the potential objects in the image, and then the lazy snapping technique delineates the wetland into the foreground. These steps were carried out using MATLAB v.2018b image processing toolbox ("MATLAB and Image Processing Toolbox 2018b"). The aforementioned steps create layers (features) such that the wetland can be discernibly identified

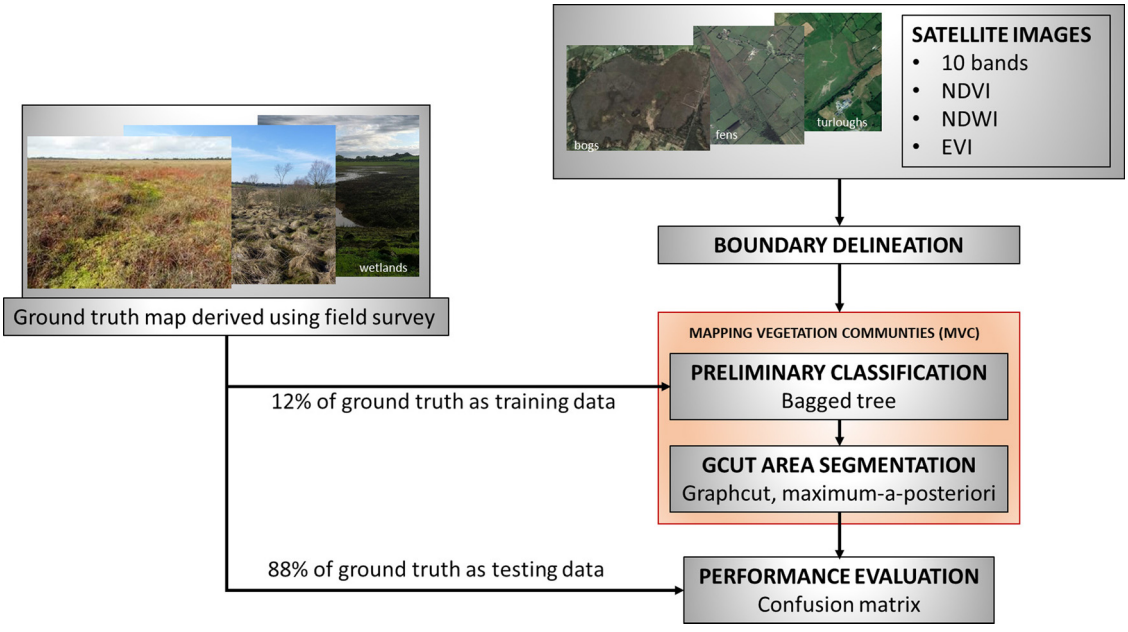


**Fig. 1.** Overall methodology used to map vegetation communities in wetlands.

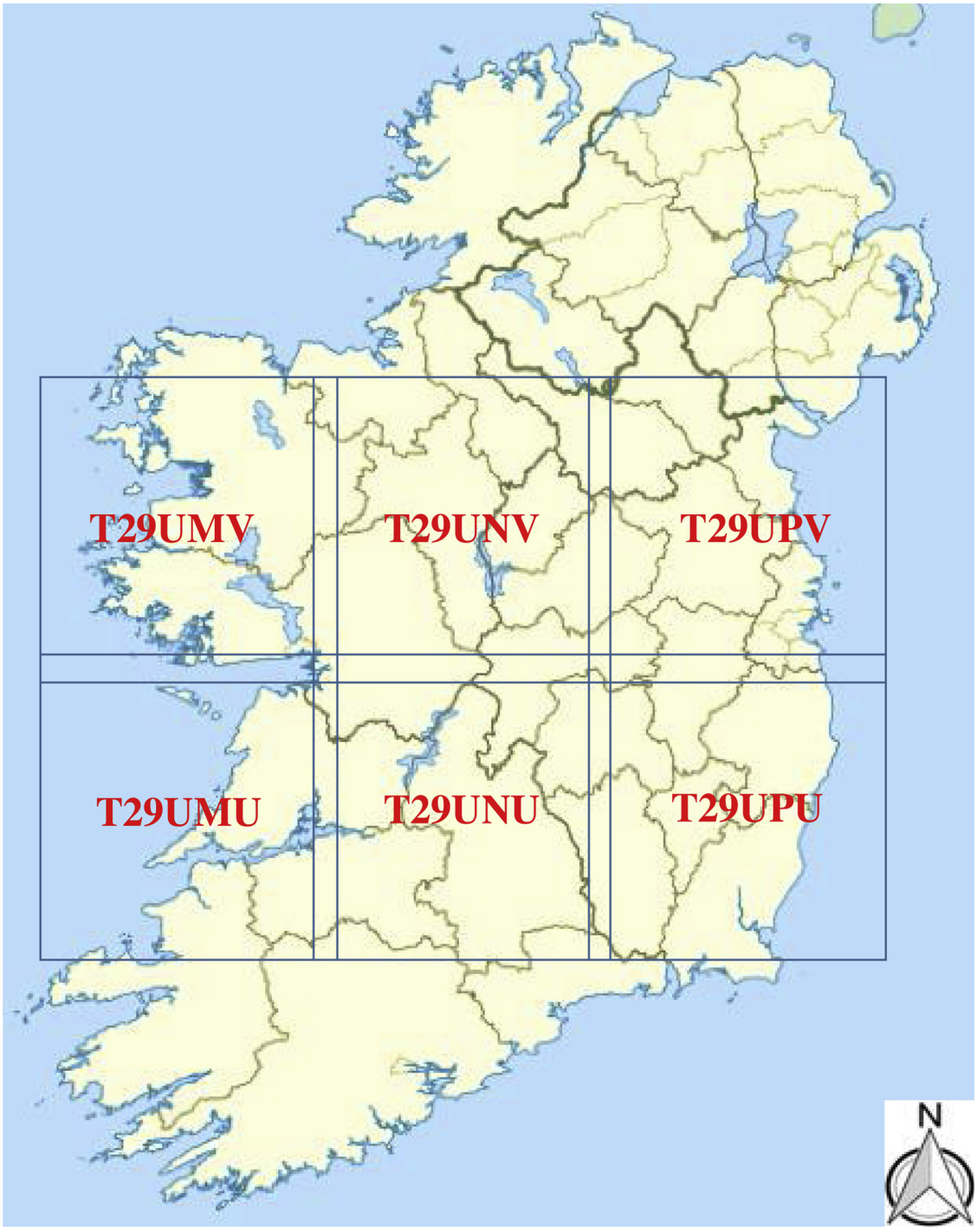


**Fig. 2.** Sentinel 2 tiles over the study areas.

**Table 2**
Sentinel 2 bands description

| BANDS | Blue | Green | Red | Veg Red Edge (VRE1) | Veg Red Edge (VRE2) | Veg Red Edge (VRE3) | NIR | Narrow NIR (NNIR) | SWIR 1 | SWIR 2 |
|---|---|---|---|---|---|---|---|---|---|---|
| Wavelength λ (μm) | 0.49 | 0.56 | 0.665 | 0.705 | 0.740 | 0.783 | 0.842 | 0.865 | 1.610 | 2.20 |
| Spatial Resolution (m) | 10 | 10 | 10 | 20 | 20 | 20 | 10 | 20 | 20 | 20 |

(Bhatnagar et al., 2018). It must be noted that this technique is useful for the delineation of bogs and fens, however, turloughs are much harder to distinguish. The turloughs' boundary lacks consistency based on the season and therefore, the delineation was carried out using the ground truth shapefiles, which were field-surveyed manually by a team of ecologists at NPWS, Ireland (NPWS, 2019). Further in this study, the 3-dimensional image of size $a \times b \times u$ was transformed into a 2-dimensional image using Eqn 1,

$$a \times b = n \tag{1}$$

**Table 3**
List of vegetation and water index used for mapping

| Index | Formula | Key significance |
|---|---|---|
| NDVI (Liu and Huete, 1995) | $NDVI = (NIR - Red)/(NIR + Red)$ | $1 \geq$ NDVI $> 0.1$ represents the presence and status of vegetation. |
| EVI (Gao et al., 2000) | $EVI = 2.5 \times (NIR - RED) / ((NIR + 6.0 \times RED - 7.5 \times BLUE) + 1.0)$ | $0.8 \geq$ EVI $\geq 0.2$, improves NDVI on high leaf area index (LAI) or chlorophyll. |
| NDWI (Gao, 1996) | $NDWI = (NNIR - SWIR1) / (NNIR + SWIR1)$ | NDWI $\geq 0.5$ detects open water and ranges much lesser for vegetation. It highlights soil moisture and wet-vegetation communities. |

with the final delineated image represented as $I^{n \times u}$, where $u = 13$ (number of bands) and $n$ is the number of pixels ($a \times b$). The 10 spectral bands, NDVI, EVI, and NDWI were used as features (layers) in this study and were defined in a feature space $\boldsymbol{U} = \{(n, u)\}$.

### 3.3. MAPPING VEGETATION COMMUNITIES (MVC)

The MVC algorithm is based on the GCut and BT classification algorithms. The steps of the MVC algorithm are described below. The algorithm was written using MATLAB v.2018b ("MATLAB 2018b").

#### 3.3.1. Step (0) Preliminary classification

For performing classification, multiple state of the art classifiers were tested for a given dataset. The ground truth was sampled randomly into training [$\boldsymbol{Z}$] (12%) and testing [$\hat{\boldsymbol{Z}}$] (88%), the training data containing a mixture of uniformly distributed data from each class.

The set of classifiers include two kernel based classifiers: (i) a SVM classifier, used with radial basis function (RBF) kernel (Cortes and Vapnik, 1995) and Naïve Bayes (Rish, 2001) with Gaussian kernel and (ii) a Euclidean distance based classifier: k-Nearest Neighbour (kNN) with k = 2 (Guo et al., 2003). Two ensemble classifiers were also compared: (i) Bagged Tree (BT) (Bauer and Kohavi, 1999), and (ii) Random Forest (RF) (Liaw and Wiener, 2002) with 30-subspaces each.

The classifier giving the best accuracy was chosen for further analysis. Table 4 presents a comparison of the classifiers (for the Clara bog dataset) for different criteria, namely model (algorithm) accuracy (5-fold validation accuracy), misclassification cost (based on 0 for correct and 1 for incorrect classification across the 8000 random pixels), prediction speed (number of observations predicted per second), and training time (the amount of time the classifier took for training in seconds).

From Table 4, the Bagged Tree (BT) classifier was chosen as the preliminary classifier for this study, based on its high validation accuracy, low misclassification cost and fast training time. Results from all the BT subspaces were averaged to make a final classification map, called [$\boldsymbol{F}(k)$], containing $n$ classified pixels of $k$ number of classes.

#### 3.3.2. Step (1) Likelihood estimation

In the next step, the likelihood related to every pixel is determined. For the image $I^{n \times u}$ and feature space $U$, the posterior probability can be defined as $Pr(F|U, I)$ (Jackson and Ragan, 1975). For the given posterior probability, the MAP estimate is given by Eqn 2(Veksler and Zabih, 1999):

$$argmax_F \left(\Pr(U, IF)\Pr(F))\right) \tag{2}$$

where $Pr(U, I|F)$ is the likelihood function and $Pr(F)$ is the prior over the classes in $F$.

#### 3.3.3. Step (2) Data and smoothness function

In this step the data and smoothness function for $U \in I^{n \times u}$ is calculated. The data function $D^{n \times k}(p_k, U)$ measures the cost of assigning the classified label $p_k$ to the pixel $p$ for a given feature space $U$ in the image $I^{n \times u}$. $D^{n \times k}(p_k, U)$ can be expressed following Boykov et al., 2001:

$$D^{n \times k}(p_k, U) = ||U(p_k) - R(p)||^2 \tag{3}$$

where $R(p)$ is the observed reflectance intensity vector of the $p^{th}$ pixel.

In this study, neighbouring pixels were encouraged to have the same class using a smoothness regularisation function $V_{p,q}{}^{k \times k}(p_k, q_k)$. This signifies the cost of assigning the classified label $p_k, q_k$ to adjacent pixels $p, q$ and was used to impose spatial smoothness. It is defined using the Potts model (Chen et al., 2007, Boykov et al., 2001) as follows:

$$V_{p,q}{}^{k \times k}(p_k, q_k) = c \times exp\,(-\Delta(p, q)/\sigma) \times T(p_k \neq q_k) \tag{4}$$

where $\Delta(p, q) = |R(p) - R(q)|$ denoting the difference in the reflectance value vector of $p$ and $q$. $c$ is a smoothness factor ($c > 0$) which was determined by trial and error to be 0.75, a value that was well suited for all wetland types. $\sigma$ is used to control the contribution of $\Delta(p, q)$ to the penalty ($\sigma > 0$). The value of $\sigma$ depends on the standard

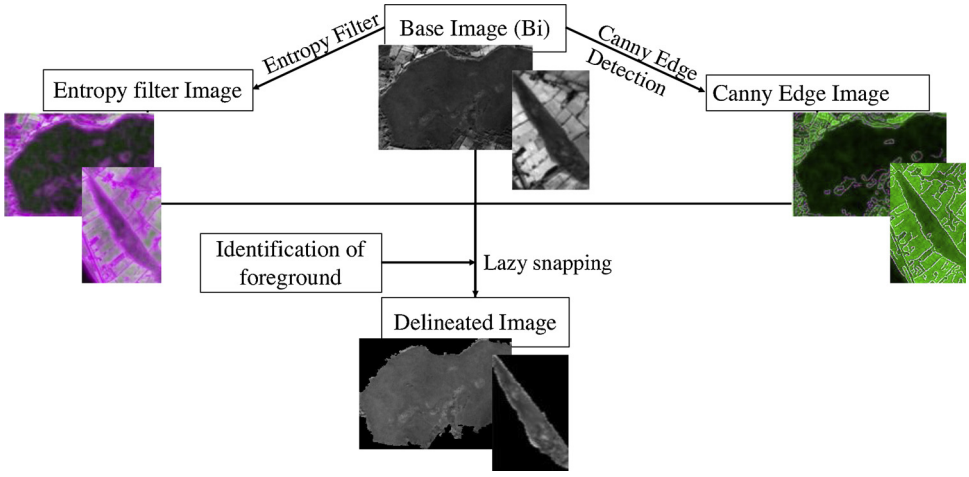


**Fig. 3.** Boundary delineation.

**Table 4**
Comparison of state-of-the-art classification techniques for Clara bog dataset

| | Model accuracy | Misclassification cost | Prediction speed | Training time |
|---|---|---|---|---|
| SVM | 78.0% | 1757 | ~ 4900 obs/sec | 23.16 s |
| kNN | 74.8% | 2017 | ~13000 obs/sec | 04.22 s |
| Naïve bayes | 71.5% | 2283 | ~ 880 obs/sec | 43.96 s |
| BT | 80.4% | 1567 | ~ 21000 obs/sec | 08.74 s |
| RF | 78.3% | 1976 | ~ 42000 obs/sec | 10.26 s |

deviation of the neighbouring pixels ($p$, $q$): the larger $\Delta$ between two neighbouring pixels, the greater the likelihood they have to be partitioned into two separate segments (Chen et al., 2007). $T = 1$ if $p_k \neq q_k$ and 0 otherwise. $V_{p,q}{}^{k\times k}(p_k, q_k)$ was defined with respect to the number of classes ($k$) so as to maximise the gradient between the pixels of differing classes.

#### 3.3.4. Step (3) Energy minimisation using $\alpha$ -expansion

The posterior maximising can be interpreted as energy (loss) minimisation (Boykov et al., 2001). The energy function was defined using Eqn 5. The $\alpha$ -expansion min cut based integer optimisation algorithm was used for minimising energy (Boykov et al., 2001; Li et al., 2011).

$$E(p_k, U) = \sum_{p\in n} D^{n\times k}(p_k, U) + \sum_{p,q\in n} V_{p,q}{}^{k\times k}(p_k, q_k) \quad (5)$$

#### 3.3.5. Step (4) Forming discrete segments

The final step is the comparison of energies of each pixel calculated in step 3 with its surrounding pixels. The pixels are classified such that the energy is minimised i.e., the maximum posterior probability per class per pixel is maintained. The loop (steps 3 and 4) continues until all the pixels are agreed upon and discrete segments are formed (using α-expansion). The final mapped image is defined by $[\hat{\boldsymbol{F}}(k)]$.

### 3.4. Performance Evaluation

Field surveys were commissioned by ecologists in the National Parks and Wildlife Service (NPWS) which were made available for analysis and mapping (NPWS, 2019). These field-derived maps were used as the ground truth (GT) in this study. It must be noted that the MVC algorithm was carried out for all the dates using training data $[\boldsymbol{Z}]$ located at the same location. The final image $[\hat{\boldsymbol{F}}(k)]$ was then validated against the testing data $[\hat{\boldsymbol{Z}}]$. The confusion matrix was used as an accuracy measure with the rows representing the ground truth and the columns representing the predicted classes by the MVC algorithm. Precision and sensitivity along with the overall accuracy (OA %; Eqn. 6) and kappa (κ) was also calculated for every vegetation community present in all the wetlands (Labatut and Cherifi, 2012).

$$OA = \frac{[TP]}{[TP + FP + FN + TN]} \quad (6)$$

where $TP$ = true positive, $FP$ = false positive, $FN$ = false negative, $TN$ = True negative

## 4. Case Studies

The MVC algorithm is validated for a total of 13 wetlands over the period of June 2017-October 2018, from which this study features three case studies as illustrative examples (see locations in Fig. 4).

For mapping, the spectral signature of the vegetation communities present in the wetlands, the S2 image, and the ground truth maps were overlaid. Only pure pixels belonging to the vegetation communities were selected. The median reflectance value for every community was plotted against the wavelengths under consideration (Figs. 5,7,9). In this study, the S2 image spectra was analysed at specific wavelengths set out in Table 2. The detailed discussion of spectral signatures at each wetland site along with the MVC algorithm results is discussed in the subsections below.

### 4.1. CASE STUDY 1 – CLARA BOG

The key ecotopes in Clara bog are based on a vegetation classification system developed by the NPWS to characterise the different conditions of a bog from the ecologically pristine active raised bog (ARB) down to a degraded status, are the Central ecotope, Subcentral ecotope, Active Flushes and soaks, Submarginal ecotope, and Marginal ecotope. Actively accumulating peat conditions occur within the Central and Subcentral ecotopes, which are generally located at the centre of the bog (Van der Schaaf and Streefkerk, 2002). Along with the Central and Subcentral ecotope areas, Active Flush areas have focused surface water flow with typically perennially wet conditions which are dominated by bog mosses (Van der Schaaf and Streefkerk, 2002; Mackin et al., 2017). In contrast, Marginal and Submarginal ecotopes, are characterised by dry vegetation communities (Van der Schaaf and Streefkerk, 2002).

#### 4.1.1. Spectral Profile

The spectral signature of Clara bog can be seen in Fig. 5 where the dissimilarity between the Central and Marginal ecotope is notable. The wetness of Central, Subcentral and Active Flush ecotopes is evidenced by the low reflectance value in the SWIR wavelengths. From Fig. 5, the Submarginal and Marginal ecotopes have similar reflectance values in NIR wavelengths but they can be distinguished by the SWIR wavelengths. The higher reflectance value of the Marginal ecotope in SWIR wavelengths depicts its dry nature. In general, the reflectance for wavelengths greater than 1300 nm is inversely proportional to the amount of water content present in the plant (Ng et al., 2007). This is also dependent on the leaf thickness of the plant.

#### 4.1.2. Vegetation Mapping in Clara Bog

The results obtained for Clara bog for the year 2017, 2018 using the MVC algorithm are presented in Fig. 6 and Table 5. In Clara bog, the Central ecotope was very well identified. This is because it is located in the wettest area of the raised bog, with indices such as NDWI giving a clear indication of its location. The Central ecotope also has a high precision value (see Table 5) which indicates that the misclassification of other communities as Central is low, justifying the above statement. The sensitivity value of the Submarginal is the highest out of all the ecotopes. However, during summer, the Subcentral ecotope starts to dry and integrate into Submarginal increasing false negatives (FN).

The Marginal ecotope is under segmented in images from 2017 and early 2018 but is identified well in summer 2018 (Fig. 6), which was one of the driest summers in Ireland in over 30 years. It can be inferred that the degraded but vegetative part of the bog (Marginal ecotope) can be best identified in a dry environment using S2 images. The OA for Clara bog ranges from 81% to 87% for all the seasons, and for all seasons the crucial ecotopes such as Central, Subcentral were picked out accurately.

### 4.2. CASE STUDY 2 – SCRAGH BOG (FEN)

In Scragh bog (fen), the predominant vegetation community is Rich

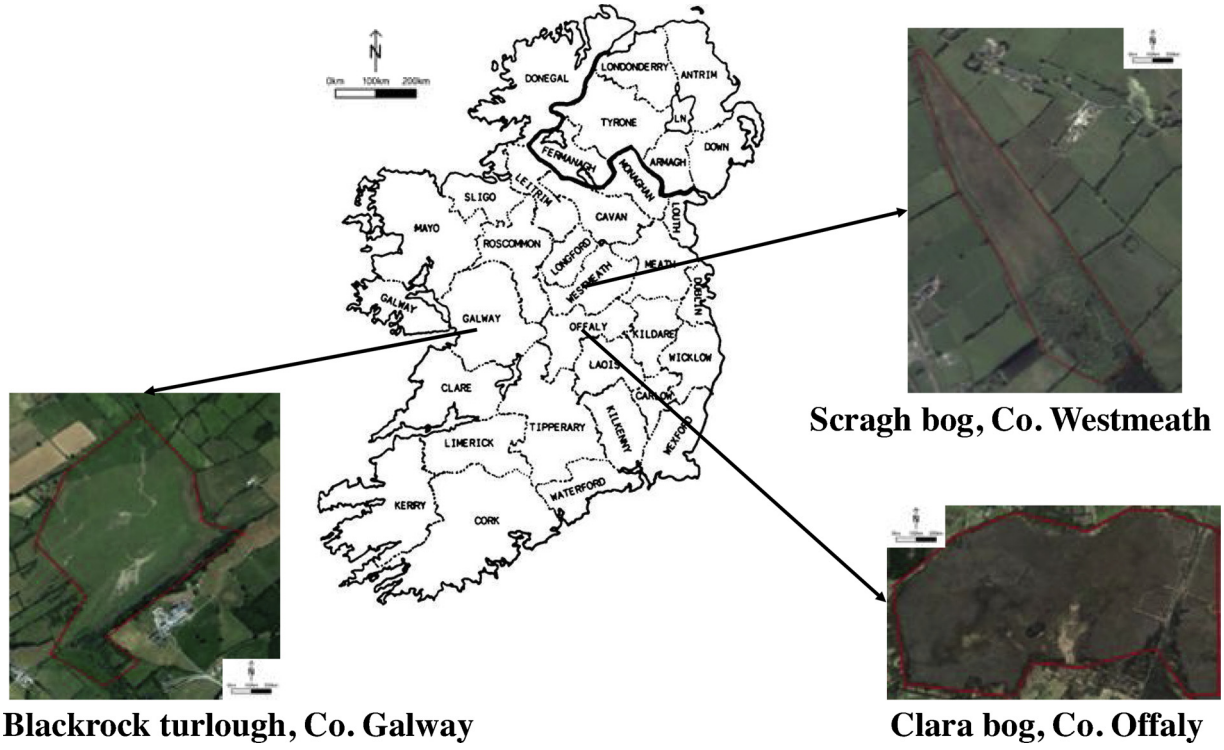


**Fig. 4.** Location of wetlands used for the case-studies in Ireland.

Fen and Transition Mire. The Rich fen communities are *Carex appropinquata*, with a range of tall herbs such as *Cirsium palustre*, *C. heterophyllum*, *Trotlius europaeus*, and *Sanguisorba officinalis* (Adam et al., 1975). The peat substrate found here is generally alkaline. The transition mires are associated with open waters and quaking bogs. This community reflects the actual succession from fen to bog (Kimberley and Coxon, 2013).. This fen also consists of non-peat forming marsh communities which are generally quite nutrient rich. Spectral Profile

Fig. 7 presents the spectral signature of Scragh bog (fen). It can be seen that the communities of wet willow-alder-ash woodland, marsh, pools, transition mires (quaking bog) and raised bog follow an overlapping pattern in the SWIR wavelengths depicting wetness in these communities. The Rich fen community, being the most nutrient-rich, has a high reflection at green and NIR wavelengths. Transition mires are generally associated with the wettest part of the fen (Foss and Crushell, 2008), which is justified with its relatively low reflectance values at SWIR wavelengths. In contrast, Conifer woodland has a high value of reflectance in SWIR wavelengths suggesting that the community is dry. This community has high reflectance at green wavelengths (band 3) which is in agreement with the visual appearance of this community.

#### 4.2.1. Vegetation Mapping in Scragh Bog (Fen)

The results obtained for Scragh bog (fen) for the year 2017, 2018 using MVC algorithm are presented in Fig. 8 and Table 6.

In Scragh bog (fen) (Fig. 8), the transition mire, an important community, has a very low FN leading to high sensitivity values (Table 6). This means that the likelihood of the misclassification of transition mires as other classes/communities is very low. Another important community, Rich fen (alkaline fen) has been identified with high precision. The actual shape of the Rich fen has been best identified in images from June 2017, 2018. This is because of the difference in wetness between transition mire and Rich fen during summer, which is picked up using NDWI. Similarly, the raised bog is identified best in the summer images (June, July, etc.), compared to the wet grasslands which are identified best in winter images. This can be attributed to the fact that during the summertime, wetness decreases and communities start to merge with the willow-alder-ash woodland community (as can

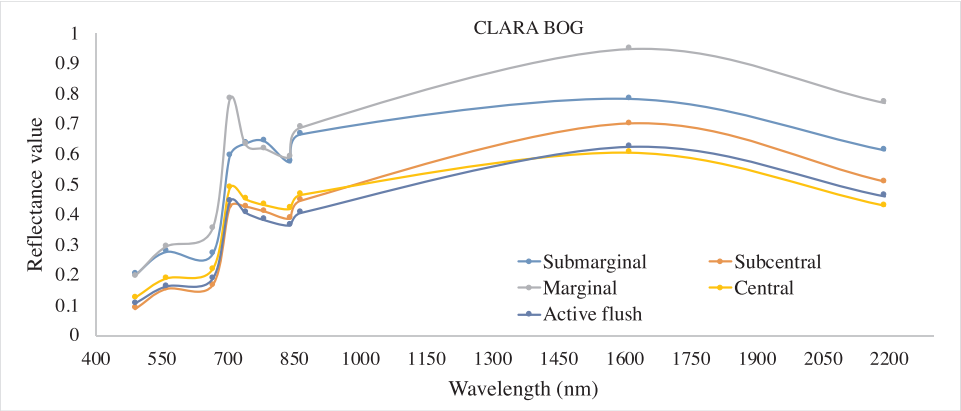


**Fig. 5.** Spectral signature of different ecotopes in Clara bog, 30th June 2018.

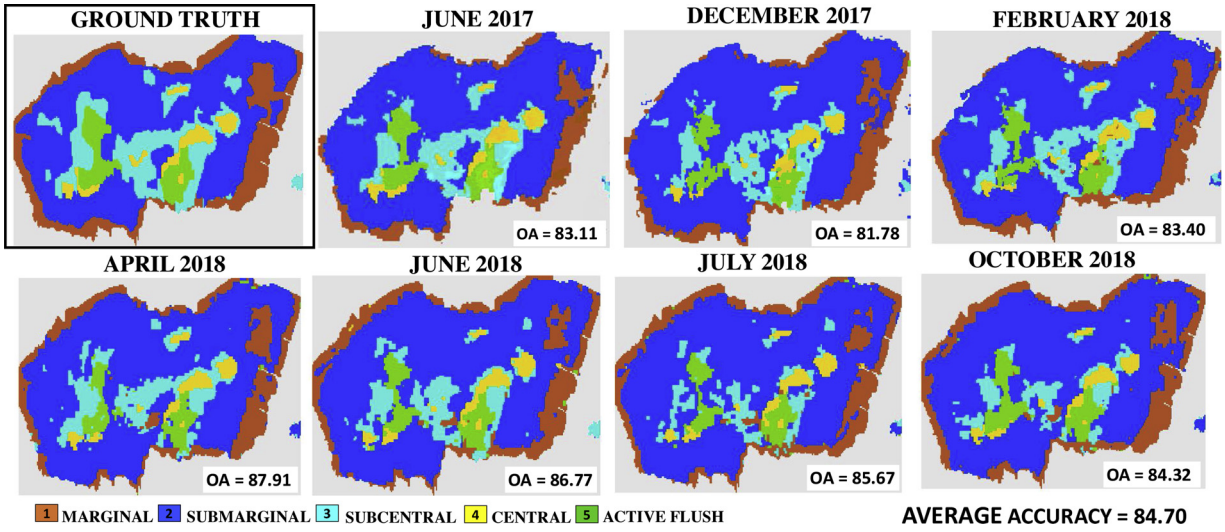


**Fig. 6.** Vegetation Communities in Clara bog for the year 2017, 2018.

be seen in Fig. 8). For the fen, the OA ranges from 82% to 84% for all the seasons, and for all seasons the crucial vegetation communities such as Rich fen community, transition mire were picked out accurately.

### 4.3. CASE STUDY 3 – BLACKROCK TURLOUGH

Blackrock turlough, under dry conditions, consists of 12 vegetation communities. These 12 vegetation communities have been agglomerated into four broad communities of the vegetation species that exist in a turlough by Waldren et al. (2015) as follows. The first broad community is formed by grouping the *Poa annua – Plantago major* community and *Eleocharis acucularis* community. The second broad community consists of *Carex nigra – Ranunculus flammula* communities and *Agrostis stolonifera – Glyceria fluitans* communities. The third broad community consist of *Agrostis stolonifera – Ranunculus repens* communities, *Agrostis stolonifera – Potentilla anserine – Festuca rubra community, Potentilla anserine – Potentilla reptans* communities, and *Fillipendula ulmaria – Potentilla erecta – Viola sp.* community. *Lolium grassland* falls is classified as another community (broad community 4) in this study. Communities such as woodland, scrubs, etc. are not a part of the broad communities and are analysed separately. Out of the four broad communities, community 4 which contains dry grassland community is the driest group whereas, community 2 is the wettest. Identification of species under these communities depicts the amount of wetness, fertility and stress tolerance of the turlough.

**Table 5**
Confusion matrix - Clara Bog, 30th June 2018 with 1. Marginal 2. Submarginal 3. Subcentral 4. Central 5. Active Flush

| CLARA | | | | | |
|---|---|---|---|---|---|
| | 1 | 2 | 3 | 4 | 5 |
| 1 | 13553 | 79 | 107 | 38 | 38 |
| 2 | 1346 | 2530 | 45 | 142 | 55 |
| 3 | 883 | 14 | 2534 | 1 | 8 |
| 4 | 43 | 73 | 0 | 772 | 54 |
| 5 | 135 | 48 | 9 | 30 | 1275 |
| Precision | 84.9 | 92.2 | 94 | 78.5 | 89.1 |
| Sensitivity | 98.1 | 61.4 | 73.6 | 81.9 | 85.1 |
| OA | 86.77 | | | | |
| κ | 0.79 | | | | |

#### 4.3.1. Spectral Profile

Fig. 9 represents the spectral signature for Blackrock Turlough. As discussed in the previous section, the species in broad community 2 show a similar vegetative pattern in visible and NIR wavelengths and overlapping pattern in SWIR wavelengths. However, the *Carex nigra-Ranunculus flammula* community has higher reflectance value in NIR wavelengths, indicating better condition of the vegetation. The vegetation species from broad community 1 differ in their spectra in vegetation red edge bands but exhibit similarity elsewhere. From the curve, the community *Filipendula ulmaria-Potentilla erecta-Viola sp. C and Potentilla anserina-Potentilla reptans* has lower reflectance in NIR

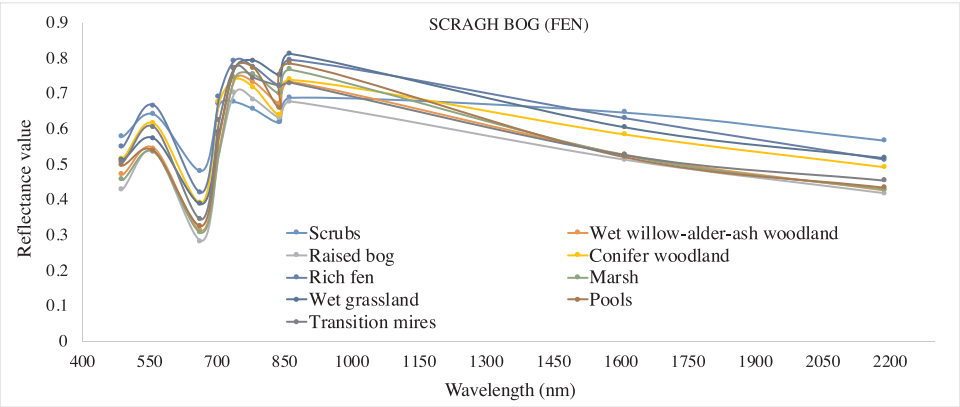


**Fig. 7.** Spectral signature of different vegetation communities in Scragh bog, 30th June 2018.

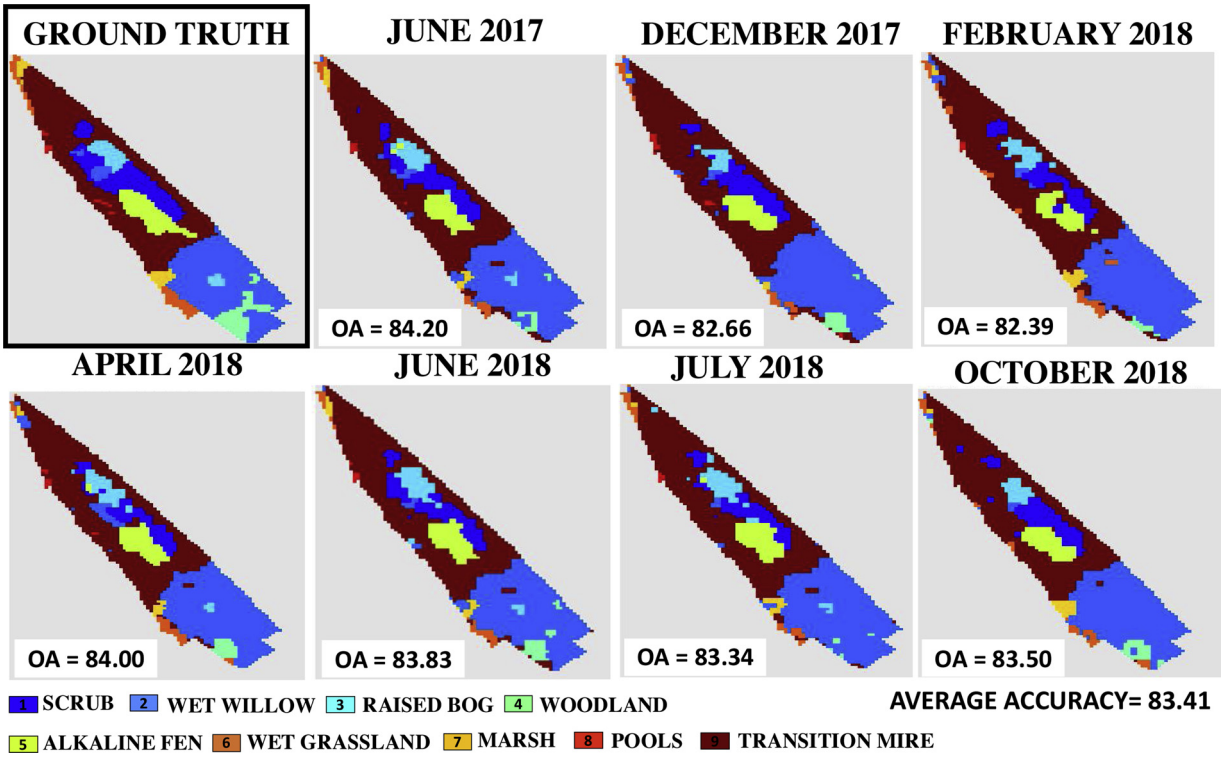


**Fig. 8.** Vegetation Communities in Scragh bog for the year 2017, 2018.

wavelengths, indicating stress. The *Lolium grassland* has higher reflectance in the NIR wavelengths depicting less stress in the vegetation and scrubs have a higher reflectance in SWIR wavelengths depicting lower water content in scrubs. This is in agreement with the field derived results stated in Waldren et al. (2015).

### 4.3.2. Vegetation Mapping In Blackrock Turlough

The results obtained for Blackrock turlough for 2017 and 2018 using MVC algorithm are presented in Fig. 10 and Table 7.

The major vegetation species present in Blackrock belong to broad community 3, *Potentilla anserina – Potentilla reptans* which is surrounded mainly by *Lolium grassland* and woodlands. It can be seen that the shape of the *Potentilla reptans* community remains intact throughout the two years with high precision and sensitivity values associated. The *Lolium grassland* also has a very high sensitivity value with a high number of true positive (TP) values which are correctly identified. This community is typically dry and not often affected by floods. The species in broad community 3 also have a high precision value of around 85%. Broad community 1 which contains ruderal species is partially identified. The species in broad community 2 are small in size but have high precision. Much of the *Agrostis stolonifera – Glyceria fluitans* community is misclassified as *Lolium grassland* hence, the low sensitivity. With small plant communities, the FN increases due to the coarse (10 m) resolution of the satellite image. Hence, it could be suggested that the small vegetation communities should be grouped and analysed as a part of a broad community using S2 images in the future. The OA for the Blackrock turlough is consistent at 84%, and for all months under consideration, the crucial communities such as *Lolium grassland*, *Potentilla reptans* were picked out accurately.

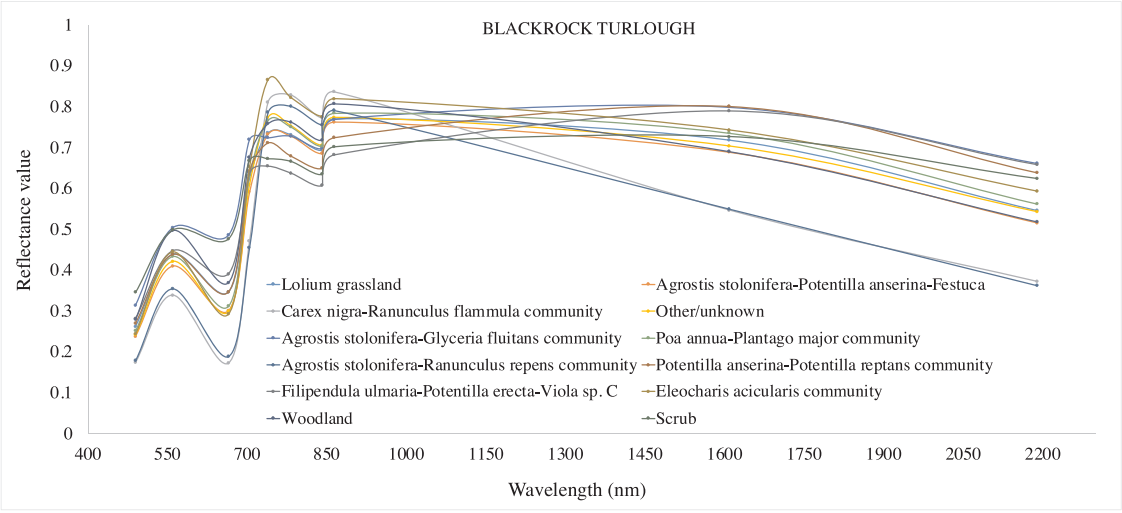


**Fig. 9.** Spectral signature of different vegetation communities in Blackrock turlough, 30th June 2018.

**Table 6**
Confusion matrix - Scragh Bog, 30th June 2018 for vegetation communities 1. Scrub 2. Wet willow 3. Raised bog 4. Woodland 5. Alkaline fen 6. Wet grassland 7. Marsh 8. Pools 9. Transition Mire

| SCRAGH | | | | | | | | | | |
|---|---|---|---|---|---|---|---|---|---|---|
| | 1 | 2 | 3 | 4 | 5 | 6 | 7 | 8 | 9 | 10 |
| 1 | 165 | 5 | 1 | 3 | 10 | 5 | 0 | 1 | 1 | 12 |
| 2 | 28 | 106 | 1 | 0 | 24 | 3 | 0 | 1 | 4 | 3 |
| 3 | 24 | 5 | 25 | 0 | 24 | 2 | 0 | 1 | 1 | 2 |
| 4 | 4 | 10 | 0 | 67 | 54 | 3 | 0 | 1 | 0 | 5 |
| 5 | 2 | 10 | 0 | 4 | 687 | 10 | 2 | 2 | 1 | 1 |
| 6 | 0 | 3 | 0 | 0 | 78 | 100 | 0 | 5 | 1 | 9 |
| 7 | 0 | 0 | 0 | 0 | 17 | 3 | 33 | 4 | 0 | 9 |
| 8 | 0 | 0 | 0 | 0 | 35 | 1 | 0 | 48 | 1 | 9 |
| 9 | 0 | 2 | 0 | 0 | 8 | 0 | 5 | 0 | 51 | 50 |
| 10 | 3 | 0 | 0 | 0 | 7 | 1 | 0 | 0 | 0 | 754 |
| Precision | 73 | 75.17 | 92.59 | 90.54 | 72.77 | 78.12 | 82.5 | 76.19 | 85 | 88.29 |
| Sensitivity | 81.28 | 62.35 | 29.76 | 46.52 | 95.54 | 51.02 | 50 | 51.06 | 43.96 | 98.56 |
| OA | 79.62 | | | | | | | | | |
| κ | 0.68 | | | | | | | | | |

## 5. Discussion

The proposed methodology illustrates the use of open-source, mid-resolution S2 data for accurately mapping vegetation communities in the bogs, fens, and turloughs. Similar studies have mainly concentrated on a single wetland-type making the application limited (Knoth et al., 2013; Crichton et al., 2015; Lehmann et al., 2016). Using the proposed generalised methodology, up to 18 vegetation communities were mapped in various wetlands, depicting its wide applicability. The mapping of the different vegetation communities can be used to infer the ecological health of the wetland, making habitat surveys simpler and more effective for ecologists. A total of 13 wetlands were mapped over time between 2017 and 2018 using the MVC algorithm. Instead of combining all the images (Rapinel et al., 2019), the study classifies each S2 image separately to monitor changes over time. The average accuracy of all the wetlands mapped is shown in Fig. 11 (more detail is provided in Supplementary Information).

The wetlands mapped in this study vary significantly in shapes and sizes, making it challenging to identify small vegetation communities using pixels at 10 m resolution. The S2-L2A imagery comes with 3 specific vegetation red-edge bands, an extra narrow NIR band that facilitates the identification of vegetation communities. To create a generalised algorithm, 10 bands of S2 imagery were insufficient, hence, 3 extra indices were used. A combination of both, NDVI and EVI, gave a clear distinction of the health of the vegetation communities present in the wetlands by measuring the chlorophyll amount and not just the greenness of the plant. To identify soil moisture content and the wetness of vegetation communities, NDWI was used which led to better overall classification of the wetland.

For the raised bog, the study was successful in mapping the key ecotopes, Central, Active Flush, and Subcentral, which indicate the peat-forming areas within the bog along with the additional ecotopes. A total of up to 9 ecotopes were mapped using the proposed algorithm. The Central and Active Flush ecotope remains predominantly wet throughout the year. The usage of NDWI index makes these communities distinguishable from Subcentral, Submarginal and Marginal. The Marginal ecotope is the greener area making the NDVI index useful in its identification. The overall results prove that MVC algorithm presented in this study provides a promising solution for automatic field monitoring of these ecotopes.

For the limestone groundwater fed wetlands, such as fens, the main challenge was to identify the transition zones such as the transition

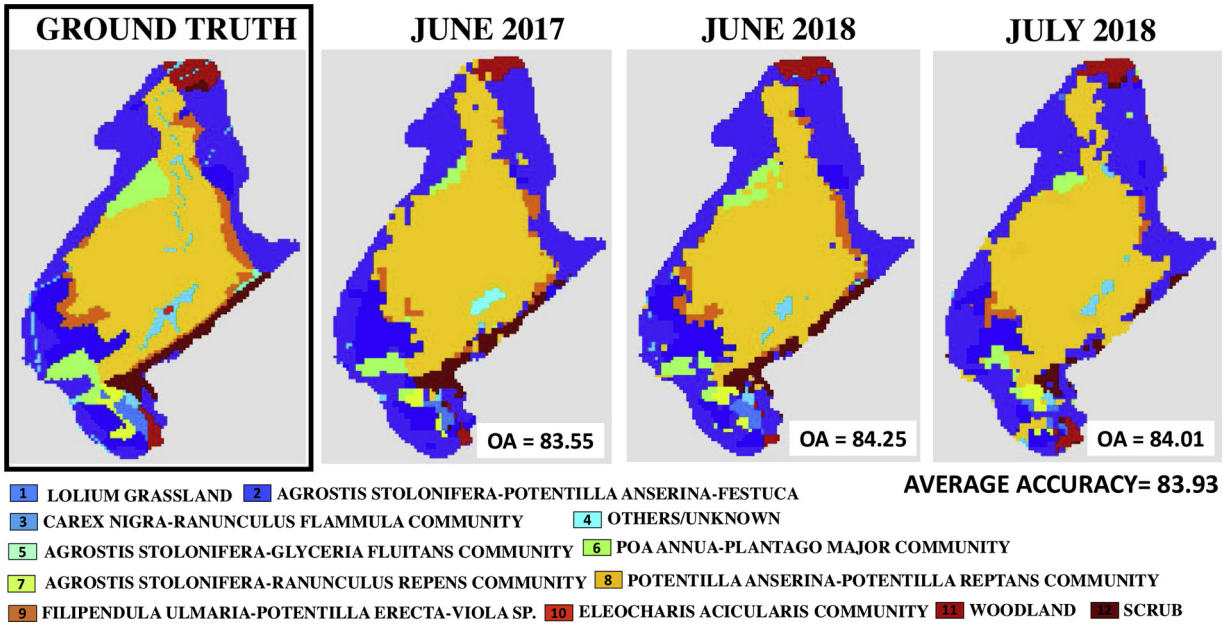


**Fig. 10.** Vegetation Communities in Blackrock turlough for the year 2017, 2018.

**Table 7**
Confusion matrix – Blackrock Turlough, 30th June 2018 for vegetation communities 1. Lolium grassland 2. Agrostis stolonifera – Potentilla anserine – Festuca rubra 3. Carex nigra – Ranunculus flammula 4. Unknown community 5. Agrostis stolonifera – Glyceria fluitans 6. Poa annua – Plantago 7. Agrostis stolonifera – Ranunculus repens 8. Potentilla anserine – Potentilla reptans 9. Filipendula ulmaria – Potentilla erecta – Viola sp. 10. Eleocharis acicularis 11. Woodland 12. Scrub

| Blackrock | | | | | | | | | | | | |
|---|---|---|---|---|---|---|---|---|---|---|---|---|
| | 1 | 2 | 3 | 4 | 5 | 6 | 7 | 8 | 9 | 10 | 11 | 12 |
| 1 | 1458 | 12 | 0 | 2 | 0 | 6 | 0 | 38 | 5 | 0 | 7 | 8 |
| 2 | 71 | 413 | 0 | 0 | 0 | 3 | 9 | 33 | 11 | 0 | 7 | 0 |
| 3 | 7 | 2 | 49 | 2 | 0 | 0 | 10 | 1 | 0 | 0 | 0 | 0 |
| 4 | 37 | 1 | 0 | 45 | 0 | 0 | 0 | 110 | 1 | 0 | 12 | 2 |
| 5 | 12 | 0 | 0 | 0 | 3 | 0 | 0 | 0 | 2 | 0 | 0 | 4 |
| 6 | 33 | 14 | 0 | 0 | 0 | 207 | 1 | 67 | 0 | 0 | 0 | 0 |
| 7 | 10 | 0 | 5 | 0 | 0 | 1 | 50 | 4 | 0 | 0 | 0 | 5 |
| 8 | 64 | 21 | 0 | 4 | 0 | 7 | 0 | 2268 | 10 | 0 | 2 | 4 |
| 9 | 53 | 7 | 0 | 0 | 0 | 0 | 0 | 69 | 174 | 0 | 0 | 13 |
| 10 | 0 | 0 | 0 | 4 | 0 | 0 | 0 | 3 | 0 | 0 | 0 | 0 |
| 11 | 50 | 0 | 0 | 0 | 0 | 0 | 0 | 1 | 0 | 0 | 115 | 0 |
| 12 | 41 | 0 | 0 | 1 | 0 | 0 | 0 | 18 | 2 | 0 | 0 | 188 |
| Precision | 79.4 | 87.8 | 90.7 | 77.5 | 100 | 92.4 | 71.4 | 86.8 | 85 | 0 | 80.4 | 83.9 |
| Sensitivity | 94.9 | 75.5 | 69.0 | 21.6 | 14.2 | 64.2 | 66.6 | 95.2 | 55 | 0 | 69.2 | 75.2 |
| OA | 84.2 | | | | | | | | | | | |
| κ | 0.81 | | | | | | | | | | | |

mire. The study was successful in identifying the transition areas as well as areas of raised bog within it. The use of SWIR wavelength and an additional NDWI index led to better identification of the wet communities. The transition mires (present in 2 out of 3 fen-sites) were mapped with high precision. High precision indicates low misclassification and the robustness of the MVC algorithm. A total of up to 9 communities were mapped in the 3 fen sites. Indices like NDVI and EVI led to better identification of the healthy (alkaline) area in the fen (Rich fen community) for all seasons.

Since turloughs are flooded throughout the winter period, the study was carried out using summer images of 2017 and 2018. A total of up to 18 vegetation communities were identified using the algorithm. The communities with high fertility, such as *Lolium grassland*, were present in all the turloughs. This community, although associated with dry conditions, has a higher level of nutrients and was identified with 72% average precision. EVI proved to be a better index for identifying grassland and scrubs due to its resilience towards chlorophyll saturation. Patches of water, pools, and flooded pavements were distinguished using NDWI (75% average precision). The study also suggests that the spatial extent of the different broad community groupings remain intact after seasonal flooding and can be identified using S2 imagery with high accuracy.

Fig. 11 depicts that the wetlands with the bigger area and bigger sample pixel size have better OAs. Therefore, it can be suggested that the use of high-resolution images which will provide a higher sample size for all areas even smaller communities may improve the algorithm performance. The reflectance value of the same vegetation communities differed in different wetlands. This was due to the change of S2-tile due to differing weather conditions, etc. However, the proposed MVC algorithm was robust, and resilient to these errors.

Overall, the temporal study carried out on the wetlands using the satellite data over two years doesn't indicate any major ecological changes, thereby indicating its effectiveness. The highest accuracies of about 87% for the raised bog, 84% for the fen and 84% for the turlough were achieved. The size of vegetation communities played a role in the overall classification accuracy. If the size of the vegetation community was less than 30 pixels (0.3 ha), the precision of mapping decreased, leading to a decrease in OA (for example, for the turloughs of Roo West

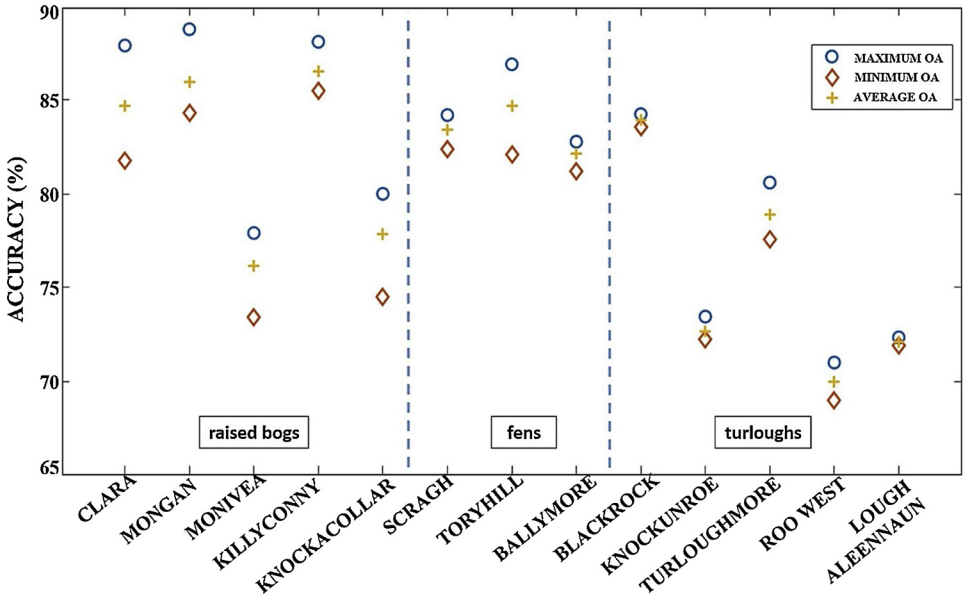


**Fig. 11.** Maximum, minimum and average accuracy (%) for all 13 wetlands.

and Lough Aleennaun). A recent study by Rapinel et al., 2019 has mapped more than 30 plant species with an average accuracy of 78% by merging the species in 7 classification communities. The present study achieved comparable OAs for mapping the small vegetation communities (< 0.3 ha) without such limitations. The OA from each wetland showed good consistency when applied to images from different times and seasons within the 2 years. This consistency in the accuracy demonstrates the robustness of the MVC algorithm and further indicates that no significant impact due to human interference or other changes has taken place in these locations, which also agrees with the reality on the ground. However, it can be assumed that if the MVC algorithm is applied to satellite images over much longer time spans, then ecological changes in the wetlands with changes in shape and size of key vegetation communities could be picked up, thereby demonstrating the effectiveness of the proposed methodology as an efficient remote monitoring tool.

## 6. Conclusion

This study successfully provides a detailed mapping of communities within wetlands using mid-resolution, open-source S2 data which has previously been carried out predominantly using expensive hyperspectral data or high-resolution data. The methodology was tested for three different types of temperate wetlands in Ireland (raised bogs, fens, and turloughs) using S2L2A images for the period of June 2017 to October 2018. In previous studies S2 data had mainly been used for classifying wetland types rather than features inside the wetlands. This study has now successfully identified both the type and extent of different vegetation communities and their subsequent area evolution with reasonable accuracy. A customised image segmentation MVC algorithm was developed by synthesising a set of existing methods to effectively and accurately segregate a set of critical vegetation communities. Vegetation indices along with soil moisture information have been used as features to train the algorithm. Individual optical bands are not capable of distinguishing different regions across the wetland and 13 layers were stacked to provide additional information to allow the classifier to perform more optimally and map more efficiently. The results provide a good characterisation of the content (S2 imagery) in both the spectral and the spatial domain. The proposed MVC algorithm has high overall accuracies for all wetlands, as well as a high precision for key vegetation communities. The novelty of the proposed methodology is that it is applicable to vegetation communities with complex boundaries of varying sizes. As shown in the study, the methodology is robust and repeatable for all seasons, all kinds of wetlands with minimal supervision. The use of this desk-based study can reduce the need for extensive field-work to a great extent, enabling ecologists to monitor the bogs using freely available satellite data. Such data can also be used to assess the progress of any restoration schemes for re-establishing the conditions in a wetland or identify potential damage (due to unlicensed drainage practices for example) which can then be used as a method of early warning for the authorities.

## Author contributions

SB, BG, SR, LG and ON conceived of the presented idea. SB, BG developed the theory and SB performed the computations, and BG, ON and LG verified the computations. The verification data was provided by SR and SW. BG, ON, SR, LG, PJ and SW contributed to the design of the research and to the writing of the manuscript.

## Acknowledgement

This study is funded by the Environmental Protection Agency of Ireland (EPAIE) (Grant No.: 2016-W-LS-13). The authors would like to thank the National Parks and Wildlife Service, Ireland (NPWS) for providing all ecological data and advice.

## References

Adam, P., Birks, H.J., Huntley, B., Prentice, I.C., 1975. Phytosociological studies at Malham Tarn moss and fen, Yorkshire, England. Plant Ecology 30 (2), 117–132. https://doi.org/10.1007/BF02389613.

Amani, M., Salehi, B., Mahdavi, S., Granger, J., 2017. Spectral Analysis of wetlands in Newfoundland using Sentinel 2A and Landsat 8 imagery. Proceedings of the IGTF. https://doi.org/10.13140/RG.2.2.34996.86407.

Amani, M., Mahdavi, S., Afshar, M., Brisco, B., Huang, W., Mohammad Javad Mirzadeh, S., White, L., Banks, S., Montgomery, J., Hopkinson, C., 2019a. Canadian Wetland Inventory using Google Earth Engine: The First Map and Preliminary Results. Remote Sensing 11 (7), 842. https://doi.org/10.3390/rs11070842.

Amani, M., Brisco, B., Afshar, M., Mirmazloumi, S.M., Mahdavi, S., Mirzadeh, S.M.J., Huang, W., Granger, J., 2019b. A generalized supervised classification scheme to produce provincial wetland inventory maps: an application of Google Earth Engine for big geo data processing. Big Earth Data 3 (4), 378–394. https://doi.org/10.1080/20964471.2019.1690404.

Bauer, E., Kohavi, R., 1999. An empirical comparison of voting classification algorithms: Bagging, boosting, and variants. Machine learning 36 (1-2), 105–139.

Bhatnagar, S., Ghosh, B., Regan, S., Naughton, O., Johnston, P., Gill, L., 2018. Monitoring environmental supporting conditions of a raised bog using remote sensing techniques. Proceedings of the International Association of Hydrological Sciences 380, 9–15. https://doi.org/10.5194/piahs-380-9-2018.

Boykov, Y., Veksler, O., Zabih, R., 2001. Fast approximate energy minimization via graph cuts. IEEE Transactions on pattern analysis and machine intelligence 23 (11), 1222–1239. https://doi.org/10.1109/34.969114.

Canny, J., 1987. A computational approach to edge detection. Readings in computer vision. Morgan Kaufmann, pp. 184–203. https://doi.org/10.1109/TPAMI.1986.4767851.

Chen, S., Cao, L., Liu, J., Tang, X., 2007. Iterative MAP and ML estimations for image segmentation. June In: Computer Vision and Pattern Recognition, 2007. CVPR'07. IEEE Conference on. IEEE. pp. 1–6. https://doi.org/10.1109/CVPR.2007.383007.

Connolly, J., 2019. Mapping land use on Irish peatlands using medium resolution satellite imagery. Irish Geography 51 (2), 187–204. https://doi.org/10.2014/igj.v51i2.1371.

Copernicus Open Access Hub, 2018. Sentinel open access hub. [ONLINE] Available at: https://.copernicus.eu. [Accessed 5 March 2018]. .

Cortes, C., Vapnik, V., 1995. Support-vector networks. Machine learning 20 (3), 273–297.

Crichton, K.A., Anderson, K., Bennie, J.J., Milton, E.J., 2015. Characterizing peatland carbon balance estimates using freely available Landsat ETM+ data. Ecohydrology 8 (3), 493–503. https://doi.org/10.1002/eco.1519.

ESA Sentinel Online, 2000. 2019. Sentinel-2 MSI Technical Guide. [ONLINE] Available at: https://sentinel.esa.int/web/sentinel/technical-guides/sentinel-2-msi. [Accessed 5 March 2018]. .

Farda, N.M., 2017. December. Multi-temporal land use mapping of coastal wetlands area using machine learning in Google earth engine. In: IOP Publishing. IOP Conference Series: Earth and Environmental Science 98. pp. 012042 No. 1.

Felicity Hayes-McCoy, W.J., 2017. Dingle and its Hinterland: People, Places and Heritage. the Collins Press, pp. 224.

Förster, M., Schmidt, T., Wolf, R., Kleinschmit, B., Fassnacht, F.E., Cabezas, J., Kattenborn, T., 2017. Detecting the spread of invasive species in central Chile with a Sentinel-2 time-series. June In: 2017 9th International Workshop on the Analysis of Multitemporal Remote Sensing Images (MultiTemp). IEEE. pp. 1–4. https://doi.org/10.1109/Multi-Temp.2017.8035216.

Foss, P.J., Crushell, P., 2008. Title: Guidelines for a National Fen Survey of Ireland, Survey Manual. Report for the National Parks and Wildlife Service. Department of the Environment, Heritage and Local Government, Ireland.

Gao, B.C., 1996. NDWI—A normalized difference water index for remote sensing of vegetation liquid water from space. Remote sensing of environment 58 (3), 257–266. https://doi.org/10.1016/S0034-4257(96)00067-3.

Gao, X., Huete, A.R., Ni, W., Miura, T., 2000. Optical–biophysical relationships of vegetation spectra without background contamination. Remote Sensing of Environment 74 (3), 609–620. https://doi.org/10.1016/S0034-4257(00)00150-4.

Gatti, A., Bertolini, A., 2013. Sentinel-2 products specification document. Available online at: https://earth.esa.int/documents/247904/685211/Sentinel-2+ Products +Specification+Document [Accessed 23 February, 2018]. .

Goodall, D.W., Gore, A.J.P., 1983. Ecosystems of the world: mires-swamp, bog, fen and moor-regional studies. Ecosystems of the world Vol. 4 Elsevierhttps://doi.org/10.1086/413982.

Gorelick, N., Hancher, M., Dixon, M., Ilyushchenko, S., Thau, D., Moore, R., 2017. Google Earth Engine: Planetary-scale geospatial analysis for everyone. Remote sensing of Environment 202, 18–27. https://doi.org/10.1016/j.rse.2017.06.031.

Grenier, M., Labrecque, S., Garneau, M., Tremblay, A., 2008. Object-based classification of a SPOT-4 image for mapping wetlands in the context of greenhouse gases emissions: the case of the Eastmain region, Québec, Canada. Canadian Journal of Remote Sensing 34 (sup2), S398–S413. https://doi.org/10.5589/m08-049.

Guo, G., Wang, H., Bell, D., Bi, Y., Greer, K., 2003. November. KNN model-based approach in classification. On the Move to Meaningful Internet Systems. Springer, Berlin, Heidelberg, pp. 986–996.

Hird, J.N., DeLancey, E.R., McDermid, G.J., Kariyeva, J., 2017. Google Earth Engine, open-access satellite data, and machine learning in support of large-area probabilistic wetland mapping. Remote sensing 9 (12), 1315. https://doi.org/10.3390/rs9121315.

Ireland's Wetlands, 2000. Irish Ramsar Wetlands Committee. Available at: www.noticenature.ie/files/Leaflet%20Web.pdf [Accessed 5 May 2018]. .

Jackson, T.J., Ragan, R.M., 1975. Bayesian decision theory and remote sensing. Photogrammetric Engineering and Remote Sensing 41 (9).

Kimberley, S., Coxon, C., 2013. Evaluating the Influence of Groundwater Pressures on Groundwater-Dependent Wetlands. STRIVE Report. online] ENVIRONMENTAL PROTECTION AGENCY. Available at: https://www.epa.ie/pubs/reports/research/water/STRIVE_100_web.pdf [Accessed 8 Aug. 2018].

Knoth, C., Klein, B., Prinz, T., Kleinebecker, T., 2013. Unmanned aerial vehicles as innovative remote sensing platforms for high-resolution infrared imagery to support restoration monitoring in cut-over bogs. Applied vegetation science 16 (3), 509–517. https://doi.org/10.1111/avsc.12024.

Koch, M., Koebsch, F., Hahn, J., Jurasinski, G., 2017. From meadow to shallow lake: Monitoring secondary succession in a coastal fen after rewetting by flooding based on aerial imagery and plot data. Mires & Peat 19. https://doi.org/10.19189/MaP.2015.OMB.188.

Labatut, V., Cherifi, H., 2012. Accuracy measures for the comparison of classifiers. arXiv preprint arXiv:1207.3790. arXiv:1207.3790v1.

Lehmann, J.R., Münchberger, W., Knoth, C., Blodau, C., Nieberding, F., Prinz, T., Pancotto, V.A., Kleinebecker, T., 2016. High-resolution classification of South Patagonian Peat Bog microforms reveals potential gaps in up-scaled CH4 fluxes by use of Unmanned Aerial System (UAS) and CIR Imagery. Remote Sensing 8 (3), 173. https://doi.org/10.3390/rs8030173.

Li, J., Bioucas-Dias, J.M., Plaza, A., 2011. Hyperspectral image segmentation using a new Bayesian approach with active learning. IEEE Transactions on Geoscience and Remote Sensing 49 (10), 3947–3960. https://doi.org/10.1109/TGRS.2011.2128330.

Li, Y., Sun, J., Tang, C.K., Shum, H.Y., 2004. Lazy snapping. ACM Transactions on Graphics (ToG) 23 (3), 303–308. https://doi.org/10.1145/1015706.1015719.

Liaw, A., Wiener, M., 2002. Classification and regression by randomForest. R news 2 (3), 18–22.

Liu, H.Q., Huete, A., 1995. A feedback based modification of the NDVI to minimize canopy background and atmospheric noise. IEEE transactions on geoscience and remote sensing 33 (2), 457–465. https://doi.org/10.1109/36.377946.

Mackin, F., Barr, A., Rath, P., Eakin, M., Ryan, J., Jeffrey, R., Fernandez Valverde, F., 2017. Best practice in raised bog restoration in Ireland. Irish Wildlife Manuals, No. 99. National Parks and Wildlife Service, Department of Culture, Heritage and the Gaeltacht, Ireland.

Mahdavi, S., Salehi, B., Granger, J., Amani, M., Brisco, B., Huang, W., 2018. Remote sensing for wetland classification: A comprehensive review. GIScience & Remote Sensing 55 (5), 623–658. https://doi.org/10.1080/15481603.2017.1419602.

Mahdavi, S., Salehi, B., Granger, J., Amani, M., Brisco, B., Huang, W., 2019. A dynamic classification scheme for mapping spectrally similar classes: Application to wetland classification. International Journal of Applied Earth Observation and Geoinformation 83. https://doi.org/10.1016/j.jag.2019.101914.

Mahdianpari, M., Salehi, B., Mohammadimanesh, F., Homayouni, S., Gill, E., 2019. The first wetland inventory map of Newfoundland at a spatial resolution of 10 m using sentinel-1 and sentinel-2 data on the google earth engine cloud computing platform. Remote Sensing 11 (1), 43. https://doi.org/10.3390/rs11010043.

Maltby, E., Acreman, M.C., 2011. Ecosystem services of wetlands: pathfinder for a new paradigm. Hydrological Sciences Journal 56 (8), 1341–1359. https://doi.org/10.1080/02626667.2011.631014.

MATLAB and Image Processing Toolbox, 2018b. The MathWorks, Inc., Natick, Massachusetts, United States.

MATLAB, 2018b. The MathWorks, Inc., Natick, Massachusetts, United States.

Millard, K., Richardson, M., 2015. On the importance of training data sample selection in random forest image classification: A case study in peatland ecosystem mapping. Remote sensing 7 (7), 8489–8515. https://doi.org/10.3390/rs70708489.

Naughton, O., Johnston, P.M., Gill, L.W., 2012. Groundwater flooding in Irish karst: the hydrological characterisation of ephemeral lakes (turloughs). Journal of Hydrology 470, 82–97. https://doi.org/10.1016/j.jhydrol.2012.08.012.

Ng, C.Q.J., Toh, Y.Y., Lam, C.Y.L., Chang, C.W., Liew, S.C., 2007. Effects of leaf water content on reflectance. 28th Asian Conference on Remote Sensing 631–636.

Nitze, I., Barrett, B., Cawkwell, F., 2015. Temporal optimisation of image acquisition for land cover classification with Random Forest and MODIS time-series. International Journal of Applied Earth Observation and Geoinformation 34, 136–146. https://doi.org/10.1016/j.jag.2014.08.001.

NPWS, 2019. Maps and Data | National Parks & Wildlife Service. [ONLINE] Available at: https://www.npws.ie/maps-and-data. [Accessed 30 April 2018].. .

Ramsar Convention Bureau, 2001. Wetlands values and functions. Ramsar Convention Bureau, Gland, Switzerland.

Rapinel, S., Mony, C., Lecoq, L., Clément, B., Thomas, A., Hubert-Moy, L., 2019. Evaluation of Sentinel-2 time-series for mapping floodplain grassland plant communities. Remote sensing of environment 223, 115–129. https://doi.org/10.1016/j.rse.2019.01.018.

Regan, S., Flynn, R., Gill, L., Naughton, O., Johnston, P., 2019. Impacts of groundwater drainage on peatland subsidence and its ecological implications on an Atlantic raised bog. Water Resources Research. https://doi.org/10.1029/2019WR024937.

Rish, I., 2001. August. An empirical study of the naive Bayes classifier. IJCAI 2001 workshop on empirical methods in artificial intelligence Vol. 3. pp. 41–46 No. 22.

SNAP - ESA, 2020. Sentinel Application Platform v6.0.5. http://step.esa.int.

Van der Schaaf, S., Streefkerk, J.G., 2002. Relationships between biotic and abiotic conditions. Conservation and restoration of raised bogs. Dept. of the Env. and Local Government, Staatsbosbeheer, pp. 186–209.

Vázquez, D.P., Atae-Allah, C., Escamilla, P.L.L., 1999. Entropic approach to edge detection for SST images. Journal of Atmospheric and Oceanic Technology 16 (7), 970–979. https://doi.org/10.1175/1520-0426(1999)016<0970:EATEDF>2.0.CO;2.

Veksler, O., Zabih, R., 1999. Efficient graph-based energy minimization methods in computer vision.

Waldren, S., et al., 2015. Turlough Hydrology, Ecology and Conservation, unpublished report. National Parks & Wildlife Services, Department of Arts, Heritage and the Gaeltacht, Dublin, Ireland.